



Lithiated Nafion membrane as a single-ion conducting polymer electrolyte in lithium batteries

Lucia Mazzapioda¹ · Francesco Piccolo¹ · Alessandra Del Giudice¹ · Laura Silvestri² · Maria Assunta Navarra^{1,3}

Received: 13 October 2023 / Accepted: 12 December 2023 / Published online: 6 March 2024
© The Author(s) 2024

Abstract

Single lithium-ion conducting polymer electrolytes are promising candidates for next generation safer lithium batteries. In this work, Li⁺-conducting Nafion membranes have been synthesized by using a novel single-step procedure. The Li-Nafion membranes were characterized by means of small-wide angle X-ray scattering, infrared spectroscopy and thermal analysis, for validating the proposed lithiation method. The obtained membranes were swollen in different organic aprotic solvent mixtures and characterized in terms of ionic conductivity, electrochemical stability window, lithium stripping-deposition ability and their interface properties versus lithium metal. The membrane swollen in ethylene carbonate:propylene carbonate (EC:PC, 1:1 w/w) displays good temperature-activated ionic conductivities ($\sigma \approx 5.5 \times 10^{-4} \text{ S cm}^{-1}$ at 60 °C) and a more stable Li-electrolyte interface with respect to the other samples. This Li-Nafion membrane was tested in a lithium-metal cell adopting LiFePO₄ as cathode material. A specific capacity of 140 mAhg⁻¹, after 50 cycles, was achieved at 30 °C, demonstrating the feasibility of the proposed Li-Nafion membrane.

Keywords Lithiated Nafion membrane · Lithium anode · Lithium polymer batteries · One step lithiation procedure · Single-ion conducting polymer

Introduction

Lead acid and lithium-ion batteries (LIBs) represent the state of the art of today's market for rechargeable batteries. Nowadays, LIBs are used in different applications ranging from consumer electronics, electric vehicles, and large-scale grid energy storage systems [1, 2]. Consequently, the ever-increasing requirements of high performance lithium ion batteries with both higher energy and power densities, are urgent. However, in the last years, because of accidents such as the Tesla electric car battery fire, the Boeing 787 Dreamliner battery problems, Samsung Note 7 fires

and explosions [3], sustainability and safety requirements became mandatory.

Current LIBs use a mixture of linear and cyclic alkyl carbonate-based liquid electrolytes which are flammable and corrosive making them unstable and unsafe. Their substitution with solid polymer electrolytes (SPEs) can be considered a valuable solution for enhancing the safety and the energy density of the next-generation LIBs, thanks to their good flexibility, no-leakage, less-flammability, and light weight.

Furthermore, they can reduce or, even prevent, the growing of dendrites on lithium metal anodes, ensuring the safety of batteries for prolonged charge/discharge cycling [4, 5].

However, the field of polymer electrolytes is an emerging class of solid-state ionic conductors (SSICs), which need to be explored. A polymer system to be used as electrolyte in lithium-ion batteries must satisfy several requirements such as high ionic conductivity ($> 10^{-4} \text{ S cm}^{-1}$) at room temperature, high chemical, thermal and mechanical stabilities, good electrode–electrolyte interface. Nowadays, these polymer electrolytes suffer from important limitations compared with traditional liquid electrolytes. The low ionic conductivity of these systems ($< 10^{-4}$ at

✉ Maria Assunta Navarra
mariassunta.navarra@uniroma1.it

¹ Department of Chemistry, Sapienza University of Rome, Piazzale Aldo Moro 5, 00185 Rome, Italy

² Dipartimento di Tecnologie Energetiche e Fonti Rinnovabili, ENEA C.R. Casaccia, Via Anguillarese 301, 00123 Rome, Italy

³ Hydro-Eco Research Center, Sapienza University of Rome, Via A. Scarpa 16, 00161 Rome, Italy

room T) and the poor compatibility in electrode–electrolyte interfaces, which result in unstable cycle stability, are not suitable for lithium-ion battery applications [6, 7].

To be competitive within the energy market, the aforementioned issues must be solved. In this context, lithiated ion-exchange membranes, such as perfluorinated sulfonic membranes, can be considered an interesting approach for developing future polymer electrolytes, due to their single-ion property which facilitates fast Li^+ transport and guarantees a Li^+ transference number equal to one [8, 9]. Moreover, this type of membranes does not require the addition of unstable and corrosive lithium salts (e.g., LiPF_6 , LiBF_4 , LiClO_4) used to promote Li ion mobility, optimizing the electrolyte conductivity. This allows also to reduce the overall cost of the battery cell [10].

In this context, Nafion membrane (DuPont), currently used as electrolyte in low temperature fuel cell devices, is one of the most common and commercially available perfluorinated ion-exchange membranes, thanks to its excellent features such as ionic conductivity under fully hydrated conditions, high thermal, and mechanical stabilities [11, 12]. One of the most noticeable characteristics of Nafion membranes is that they are single-ion conductors; they can transfer cations selectively due to the presence of sulfonic groups ($-\text{SO}_3^-$ anions) covalently bonded to the polymer chains and unable to move through the membrane, avoiding the detrimental effect of anion polarization during cell operation [13, 14]. However, Nafion membranes, being proton-conductive, need a lithiation process, before using them as electrolyte in LIBs.

The most common procedure to prepare lithiated Nafion membranes is based on the use of 1 M lithium hydroxide (LiOH) solution to convert H-Nafion membrane in the lithium form [15–17]. Nevertheless, this method allows to exchange only a limited number of protons, resulting in low ionic conductivity obtained for the lithiated membranes.

In this paper, we propose a novel synthesis route for lithiated-Nafion membrane, based on a single-step solvent casting method, where both the preparation and lithiation processes of the Nafion membrane occur at the same time. Physical–chemical characterizations of both H-Nafion and Li-Nafion membranes were carried out through a multi-level approach by small and wide-angle X-ray scattering (SAXS-WAXS), Fourier transform infrared spectroscopy (ATR-FTIR), and thermogravimetric analysis (TGA). The electrochemical stability window analysis and the ionic conductivity of the Li-Nafion membrane were investigated by adopting non aqueous solvents as swelling media. The electrolyte with better electrochemical results was studied in a secondary cell using LiFePO_4 (LFP) as cathode material and lithium metal as anode.

Results and discussion

Lithiated Nafion (Li-Nafion) membranes were prepared by following a novel one-step casting procedure where the preparation and lithiation of the membrane occur simultaneously. In detail, lithium hydroxide was dissolved at 80°C into a commercial Nafion (E.W. 1100) solution at a 5 wt% concentration with respect to the dry Nafion content. Subsequently, solvents were replaced with *N,N*-dimethylacetamide and the final mixture was casted and dried on a Petri dish. In this way, we obtained a Li-Nafion membrane with a homogeneous thickness around $60\ \mu\text{m}$, as observed from SEM images in Figure S1.

These membranes were compared with the H-Nafion membranes prepared with the common procedure described in the experimental section.

Small-angle and wide-angle X-ray scattering (SAXS-WAXS) studies have demonstrated that Nafion membrane is structured in a three-phase system consisting of (1) an inhomogeneous polymer matrix at the tens of nanometer scale, (2) the ion clusters with characteristic spacings in the order of a few nm, and (3) a crystalline phase with periodic inter-atomic distances below 1 nm [18]. All these phases are recognized in a SAXS-WAXS plot by the relative peaks, namely the matrix knee, the ionomer peak, and the “crystalline” peaks respectively. As reported in the literature for the H-Nafion membranes, the matrix knee corresponds to the size and correlation distances of the more electron-dense fluoro-carbon polymer crystallites distributed in the amorphous polymer matrix and this feature depends on the processing conditions but remains almost unchanged between dry and water-swollen membranes because of its hydrophobic nature. The ionomer peak is related to the local ordering of the ionic domains within the polymer matrix, in which the water is contained. Thus, the position and intensity of this peak are correlated with the hydration degree of the Nafion membrane. The last two crystalline peaks are due to interatomic spacings of the Nafion structure which has a well-known degree of crystallinity, providing the structural integrity and mechanical stability of the membrane [19, 20].

In Fig. 1, the SAXS-WAXS plot of a Li-Nafion membrane is compared with that of an H-Nafion sample. As visible, all the above-described peaks are recognized in both Nafion membrane profiles. However, the lithiation procedure seems to lead a re-organisation of amorphous structure of the polymer as visible from the diminished intensity of both the matrix knee and ionomer peak in the Li-Nafion membrane. The replacement of protons with lithium seems to alter the structure of the Nafion membrane, probably due to an increased degree of cross-linking within the ionic clusters of the polymer, which

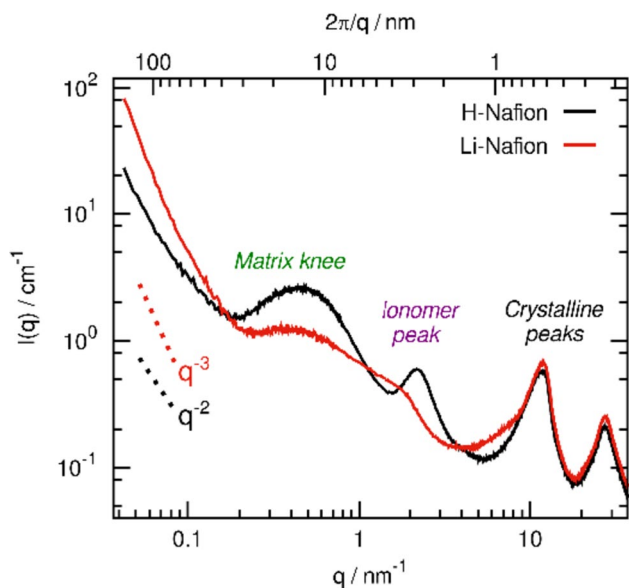


Fig. 1 SAXS-WAXS profiles of dry H-Nafion and Li-Nafion membranes

can modify the local meso-morphology of the membrane [21]. The less defined ionomer peak in the Li-Nafion membrane appears shifted to lower angles (1.8 nm compared to 2.2 nm), suggesting a more disordered clustering of the ionomer domains with larger characteristic distances (3.5 nm compared to 2.9 nm, closer to values usually observed in hydrated conditions). On the contrary, the structural peaks in the WAXS region remain largely unchanged; compared to H-Nafion, for the lithiated membrane it can be appreciated an additional broad contribution around 9 nm^{-1} to the first WAXS peak, which is possibly attributed to larger characteristic spacings within the amorphous portion of the polymer compared to the H-Nafion sample [18].

The goal of the ATR-FTIR studies of the perfluorinated ionomers was to verify the conversion of the ionomers from H^+ into Li^+ form. FTIR spectra of both hydrated Nafion membranes before (H-Nafion membrane) and after (Li-Nafion membrane) lithiation are compared in Fig. 2. As evident, the main peaks related to the Nafion structure, such as the hydrophobic fluorocarbon chains ($1300\text{--}1000 \text{ cm}^{-1}$) and the perfluoroetheral side chains ($1000\text{--}800 \text{ cm}^{-1}$), can be clearly distinguished for both samples. It is interesting to note that the peak at 1080 cm^{-1} , which is assigned to the $-\text{SO}_3$ symmetric stretch band, is shifted to high wavenumber, whereas the peak at 1710 cm^{-1} , due to the bending band of the hydrated H-Nafion membranes, is placed to 1630 cm^{-1} in the spectrum of Li-Nafion membrane. These shifts are attributed to the interaction between Li^+ ion and oxygen and confirm the exchange of protons by lithium ions, in

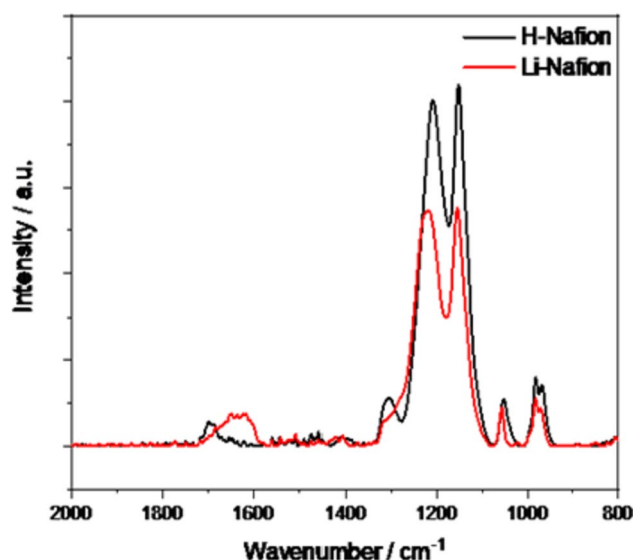


Fig. 2 ATR-FTIR spectra of hydrated H-Nafion and Li-Nafion membranes

agreement with those observed in the IR spectra of lithiated Nafion membranes already reported by other authors [16, 22, 23].

The thermal stability of both H-Nafion and Li-Nafion membranes were evaluated by TG analysis and are presented in Fig. 3. As known, the H-Nafion membrane starts to decompose just above $300 \text{ }^\circ\text{C}$, with the first weight loss being the most critical because it is attributed to the splitting-off of the sulfuric acid groups in the membrane [24, 25]. This corresponds to the loss of the ion exchange functionality. Clearly, the Li-Nafion membrane starts decomposing at temperatures higher of about $150 \text{ }^\circ\text{C}$ with respect

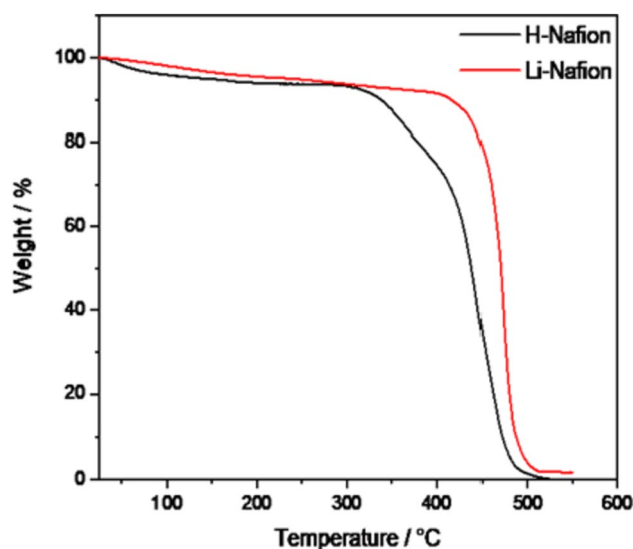


Fig. 3 TGA response of H-Nafion and Li-Nafion membranes

to H-Nafion, demonstrating a better thermal stability. This behaviour can be justified, considering a stronger bonding between oxygen and lithium in the Li-Nafion membrane compared to the interaction of oxygen with hydrogen in the H-Nafion membrane [26].

Considering the results obtained, we can conclude that the replacement of H^+ by Li^+ in the Nafion membrane through our single-step lithiation procedure was successfully achieved.

To be used as polymer electrolyte for LIBs applications, Li-Nafion membrane needs to be soaked in anhydrous mixtures of organic solvents, to induce the Li^+ ion dissociation from sulfonic groups and its mobility within the polymer matrix. In our studies, three carbonate-based solvent mixtures, i.e., EC (ethylene carbonate): PC (propylene carbonate) 1:1 wt/wt, EC (ethylene carbonate): DMC (dimethyl carbonate) 1:1 wt/wt and EC (ethylene carbonate): DEC (diethyl carbonate) 1:1.2 wt/wt, have been chosen to evaluate their effect on the performances of Li-Nafion membranes. The solution uptake % of the membrane in each solvent mixture was determined at room temperature by a gravimetric method according to the following equation [27]:

$$\text{Swelling degree (\%)} = [(M_{\text{wet}} - M_{\text{dry}})/M_{\text{dry}}] \times 100, \quad (1)$$

where M_{wet} is the weight of the fully swollen membrane after soaking the sample in the solvents for 3 days. M_{dry} is the weight of dry membranes measured after 5 h at 110 °C under vacuum. As reported in Table 1, it was observed that the solution uptake is as high as 94 wt% for the membrane swollen in EC:PC, whereas smaller values are observed for Li-Nafion swollen in EC:DMC and EC:DEC. In view of their application in lithium batteries, we have determined the lithium conduction properties of Li-Nafion membranes by EIS. Table 1 shows the ionic conductivity obtained at three temperatures of interest (i.e., 20 °C, 40 °C and 60 °C) for each sample.

All the investigated membranes possess an ionic conductivity in the order of $10^{-4} \text{ S cm}^{-1}$, which is comparable or even higher than that of most polymer electrolytes [21, 28, 29]. Clearly, the lithium conductivity of Nafion depends both on the solvent uptake and solvent nature. The good solvent

uptake of Li-Nafion swollen in EC:PC does not guarantee the highest room-T conductivity but this membrane shows the best T-dependant behaviour, with σ as high as $5.5 \times 10^{-4} \text{ Scm}^{-1}$ at 60 °C. This is probably related to the high dielectric constant and relatively low evaporations tendency of EC-PC mixture, which lead to an enhancement of ions dissociation and an improvement of Li^+ ion transport with temperature [30]. Moreover, the high content of plasticizer solvents in the EC-PC swollen membrane provides the formation of an effective cluster-network of transport channels and promotes the ion transport [31]. As known for H-Nafion membranes, the sulfonate exchange sites give rise to spherical clusters that increase their size with hydration level, allowing the ionic conductivity of Nafion membrane [32]. Generally, Grotthus (surface diffusion mechanism) and vehicle mechanisms (bulk diffusion mechanism) are involved in the proton conduction in Nafion membranes under hydrated conditions. In particular, in the Grotthus mechanism, protons attached to sulfonic acid groups, hop from one water molecule to the next one along the hydrogen-bond network, whereas in the vehicle mechanism, protons are transferred by the diffusion of H^+ species in the electrolyte [33]. It was demonstrated that the proton transport within Nafion membrane is strongly affected by water content and operating temperature. In particular, at low relative humidity, the connectivity between water molecules is poor because of the low degree of hydration of the membrane, thus the protons can be transferred within the polymer matrix by following only the vehicular mechanism, with a consequence of reducing the ionic conductivity of Nafion membrane [33, 34].

Therefore, we can assume that in the Li-Nafion membranes swollen in EC:PC the lithium transportation within the polymer matrix can be governed by both Grotthus and vehicle mechanisms, thanks to the high solvent swelling degree of the membrane, which guarantees great ionic conductivity to this sample upon the temperature increase. To be noted that conductivity values as high as $2.5 \times 10^{-3} \text{ S cm}^{-1}$ have been shown for Nafion-117 membranes in the Li^+ form [35]. In that case the membrane underwent a preliminary treatment by specific thermal methods and a subsequent conditioning in EC:PC mixtures. Even though promising for possible further improvements, in this paper energy- and time-consuming additional treatments are intentionally avoided, still preserving acceptable ionic conductivity.

The electrochemical stability window of the polymer electrolytes was determined by linear sweep voltammetry (LSV) and cyclic voltammetry (CV). In Fig. 4, the LSVs curves of each sample are reported. The electrolyte membrane swollen in EC:DMC 1:1 shows the highest stability against oxidation because no current drift up to 5 V vs Li^+/Li is observed. However, a good oxidative stability is also obtained with EC:PC Li-Nafion, displaying negligible current below 5 V.

Table 1 Swelling degree and ionic conductivity of Li-Nafion membranes swollen in EC:PC 1:1wt/wt, EC:DMC 1:1 wt/wt and EC:DEC 1:1.2 wt/wt

Solvent mixture (wt:wt)	Solvent uptake (wt%)	σ (Scm^{-1})		
		20 °C	40 °C	60 °C
EC:PC 1:1	94	2.1×10^{-4}	3.5×10^{-4}	5.5×10^{-4}
EC:DMC 1:1	68	7.7×10^{-5}	8.3×10^{-5}	2.0×10^{-4}
EC:DEC 1:1.2	68	3.9×10^{-4}	4.1×10^{-4}	4.3×10^{-4}

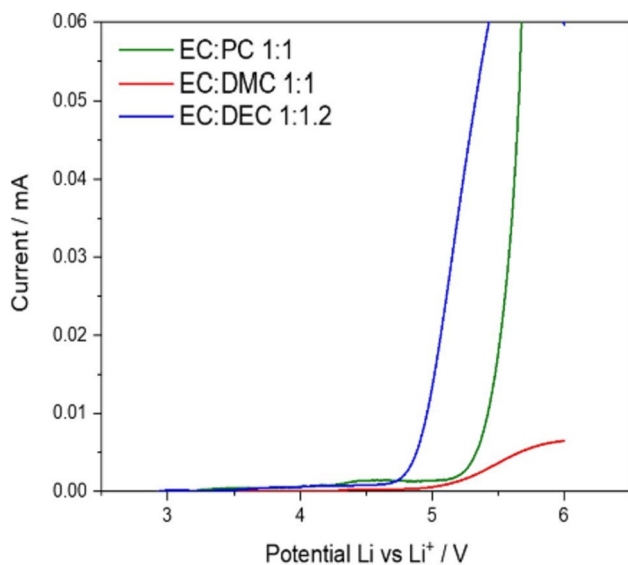


Fig. 4 LSV curves, recorded in Li||C cells, for the Li-Nafion samples swollen in EC:PC 1:1 wt/wt (green curve), EC:DMC 1:1 wt/wt (red curve) and EC:DEC 1:1.2 wt/wt (blue curve)

The cathodic stability of all Li-Nafion membranes was evaluated by CVs and reported in Fig. 5. EC:DMC and EC:DEC swollen membranes show in the first sweeping cycle a large reduction current at around 1.5 V vs Li^+/Li , associated with a decomposition process due to the reduction of the carbonate solvents and the formation of a solid electrolyte interphase (SEI) on the surface of the carbon electrode. In the following cycles, this peak disappears, confirming the formation of a stable SEI. In the first cycle of Li-Nafion membrane swollen in EC:PC, a decomposition phenomenon is revealed already at 2.5 V vs Li^+/Li . However, this process is constant until 1.5 V, suggesting that the EC and PC cyclic carbonates may have a synergistic effect on the electrolyte stability. The formation of a SEI layer is detected below 1 V vs Li^+/Li for the EC:PC swollen sample and, also in this case, subsequent cycles are observed, even though with smaller associated currents. The reduction and oxidation currents close to 0 V vs Li^+/Li are ascribed to the lithium intercalation/de-intercalation processes occurring at the working Super P carbon electrode [30, 36].

The interfacial properties between Li metal and Li-Nafion membranes were studied by means of the stripping and deposition measurements in symmetrical lithium cells (Fig. 6).

As evident, the EC:PC swollen membrane exhibits the smallest and most stable overvoltage at all applied current densities. On the contrary, in the other two samples the overvoltage increases at a larger extent with increasing the current density. The better interface between Li metal and the EC:PC Li-Nafion membrane can be justified considering both its lithium ion conductivity, which guarantees small overvoltage, and stability of the entrapped

EC:PC solvent mixture, allowing improved electrochemical response compared to the other electrolytes.

To further verify the stability of EC:PC Li-Nafion membrane in contact with lithium, we evaluated the interfacial resistance on Li | Li symmetrical cells by electrochemical impedance spectroscopy, acquiring the spectra for 4 days at open circuit voltage (OCV). Nyquist plots of the impedance spectra are shown in Figure S2a. In the high frequency region, the intersection at the Z'_{real} axis represents the ohmic resistance of the electrolyte whereas, in the medium-lower frequency region, the diameter of at least two suppressed and overlapping semicircles reflects the total interfacial resistance. The changes in the interfacial resistance during the OCV storage time are presented in Figure S2b. As reported elsewhere, the down trend occurring upon the first 6 h is typically due to the formation and deformation of SEI on the lithium surface [37]. However, after 12 h, we can observe a significant increase of the total interfacial resistance. Then, it starts to decrease and reaches a steady state after 2 days, showing a constant charge transfer due a stable electrode/electrolyte interface.

The Li-Nafion membrane swollen in EC:PC was selected to be tested as electrolyte under galvanostatic charge–discharge cycles in Li-metal cells. To this purpose, a coin cell adopting a lithium metal anode and a lithium iron phosphate (LFP) cathode, separated by the quoted membrane, was assembled. For this preliminary attempt, LFP was considered the most suitable cathode material, thanks to its well-known, very stable performance, allowing an easy evaluation of the polymer electrolyte effect on the Li|LFP cell. Moreover, LFP has great sustainability features and a relatively low nominal voltage, preventing the polymer decomposition. Indeed, the battery was expected to operate below 4 V vs. Li^+/Li , well within the stability domain of the electrolyte as demonstrated by LSV results reported in Fig. 4.

In Fig. 7, the cell voltage profile and the specific capacity as function of cycle numbers are shown. The measurement was carried out at 30 °C and $C/10$ constant current, with $1C = 170 \text{ mA g}^{-1}$.

As reported in Fig. 7, the cell shows an activated trend probably due to an activation of the Nafion electrolyte. This process of performance improvement is widely known for Nafion in fuel cell devices and it is reported as break-in [38]. In detail, a newly proton exchange membrane fuel cell (PEMFC) needs to be activated to achieve its maximum performance. Moreover, as mentioned by Nicotera et al. [21], who have already reported a similar cell behaviour with their composite lithiated Nafion membranes, an activation of the LFP material in the electrode can be assumed due to a slow wetting of the swollen membrane. Also in this case, we can suppose a non-optimized electrode–electrolyte contact, which induces to reach a

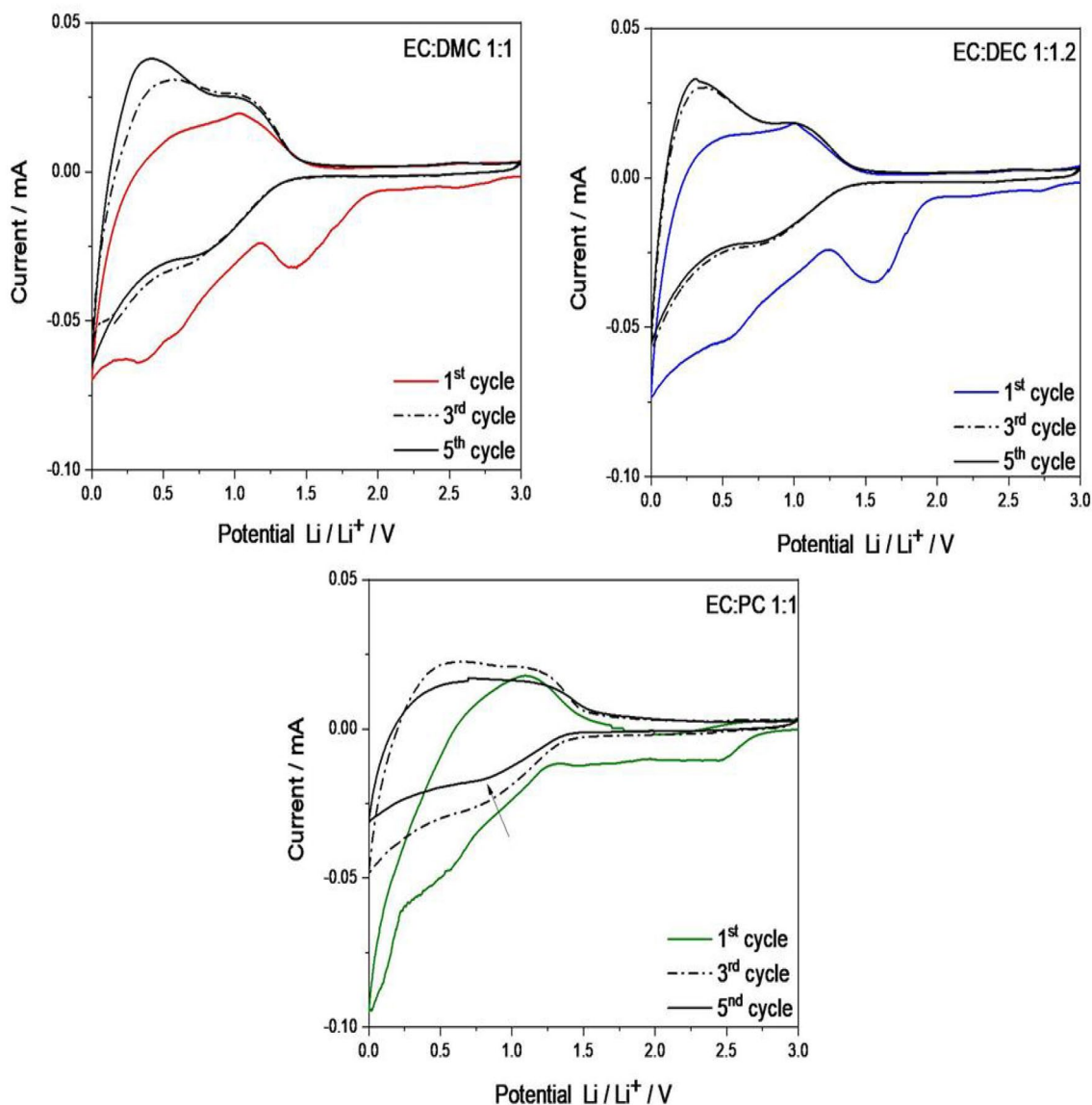


Fig. 5 CV curves, recorded in LillC cells, for the Li-Nafion samples swollen in EC:PC 1:1wt/wt (1st cycle in green), EC:DMC 1:1 wt/wt (1st cycle in red) and EC:DEC 1:1.2 wt/wt (1st cycle in blue)

stable specific capacity of about 130 mAhg^{-1} only after 20 cycles.

Due to the activated trend of LFP electrodes in lithium cells when the EC:PC Li-Nafion membrane is used, we investigated the electrode/electrolyte interface carrying out impedance measurements on the cell upon cycling. Specifically, impedance spectra were acquired at the end of cycles 1, 5, 10, 15 and 20 and the results have been reported in Figure S3.

Nyquist plots are characterized by a well-defined semicircle, starting at high frequency, and a sloping line in the low frequency region, resembling a non-blocking capacity-type nature. If compared to the spectra of Figure S1, related to a symmetrical LillLi cell stored at open

circuit, the trend shown in Figures S3 demonstrates a small bulk resistance (see the intersection with Z'_{real} axis in Figure S3b) and lower electrolyte/electrode interface resistances (see the amplitude of the semicircles in Figure S3a), indicating a good LFP/membrane electrical contact. Upon cycling, during the first 10 cycles, interfacial resistance values increase up to 4 times, whereas only a limited increase of bulk resistance is observed (from about 50 to 75Ω). Based on this, no relevant solvent leaching from the polymer is ascribed but a possible structural rearrangement of both Nafion polymer and LFP active material is recognized to affect the electrode/electrolyte interface. After the 10th cycle cell resistances start to decrease. At the 20th cycle the cell appears almost stabilized, in

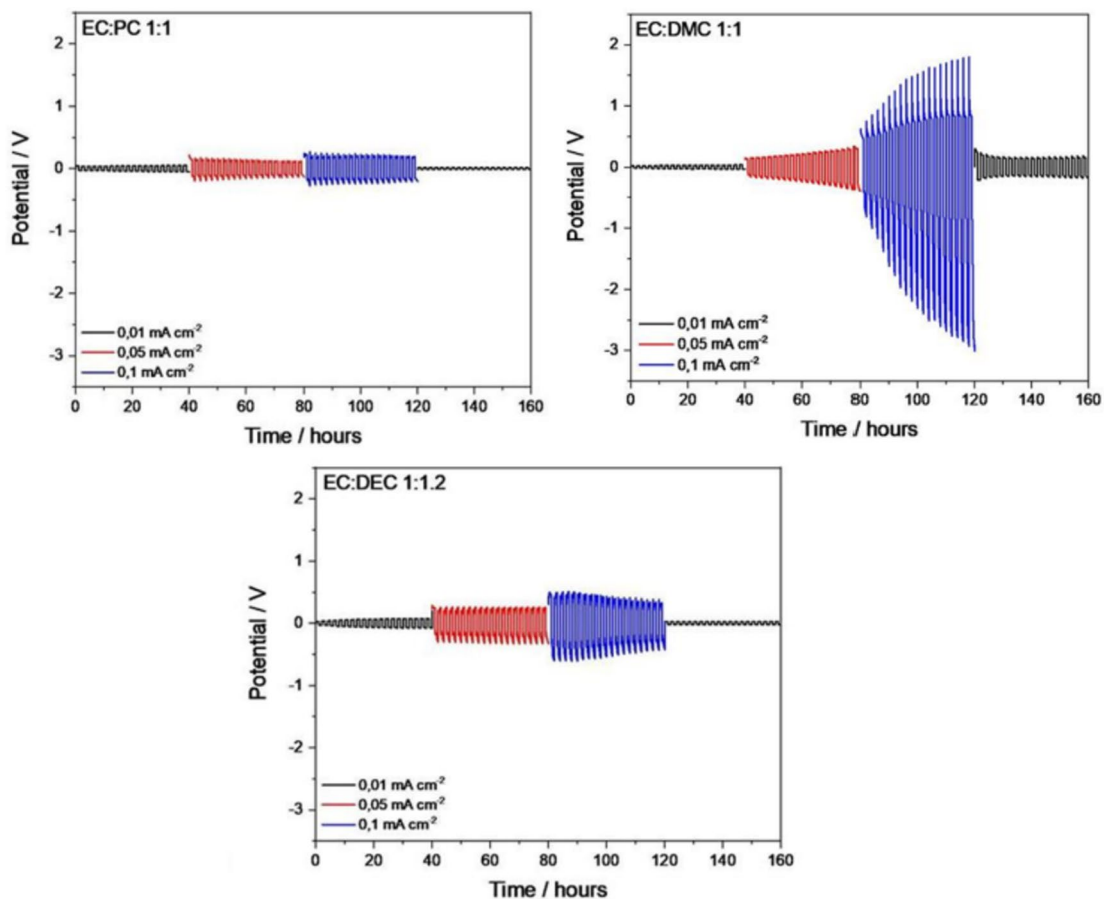


Fig. 6 Li stripping/deposition, in symmetrical Li-metal cells, for the Li-Nafion samples swollen in EC:PC (up left), EC:DMC (up right), and EC:DEC (bottom), at three different current densities: 0.01 mAcm⁻² (black), 0.05 mAcm⁻² (red), 0.1 mAcm⁻² (blue)

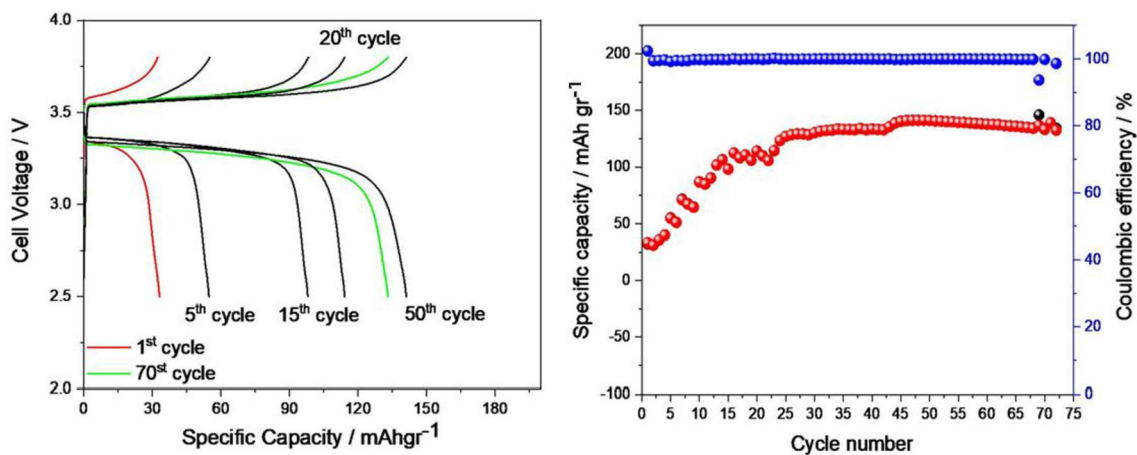


Fig. 7 Charge–discharge curves (on the left) and cycling stability at different cycle numbers (on the right) of Li|EC:PC Li-Nafion|LiFePO₄ cell at 30 °C, C-rate: 0.1 C

agreement with the capacity response of galvanostatic cycling in Fig. 7.

A possible strategy to improve the LFP/electrolyte contact and promote a faster stabilization, could be the use of the lithiated Nafion polymer also as binder instead of conventional PVDF used in LIBs. This replacement can improve the electrolyte–electrode interface, enhancing the lithium-ion transport during battery operation. Anyhow, the cell is able to supply reversible performance with a Coulombic efficiency up to 100% and a specific capacity of about 140 mAhg^{-1} at the 50th cycle, which is close to the nominal capacity of the LFP adopted. Unfortunately, from the 70th cycle, the discharge capacities of the cell start decreasing to 133 mAhg^{-1} probably due to an increasing of interface resistance. Overall, the performances obtained with the proposed EC:PC Li-Nafion membrane in a $\text{Li}|\text{LiFePO}_4$ cell demonstrate good potentiality, strengthening the existing literature on Nafion single-ion conducting polymer electrolytes [21, 29].

Conclusion

In the present work, lithiated-Nafion membranes synthesized by a single-step method are proposed. Their applicability in LIBs as polymer electrolyte is discussed. From SAXS-WAXS, ATR-FTIR and TGA analyses the success of the proposed lithiation procedure is confirmed. The new lithium conducting membranes have been swollen in three carbonate-based solvent mixtures (EC:DMC 1:1, EC:DEC 1:1.2 and EC:PC 1:1), achieving a swelling degree close to 100 wt% with EC:PC 1:1. Ionic conductivity of the electrolytes at different temperatures has been characterized by impedance spectroscopy. Interesting T-activated ionic conductivities are obtained for the membrane swollen in EC:PC, which displays also a more stable Li-electrolyte interface with respect to the other samples and a good electrochemical stability window. The Li-Nafion membrane swollen in EC:PC 1:1 has been successfully used as electrolyte in a $\text{Li}|\text{LiFePO}_4$ cell prototype, demonstrating its promising performance in galvanostatic charge–discharge tests. Even though further optimization is needed to speed up cell performance activation, it is believed that lithiated Nafion, entrapping reasonable amounts of suitable solvents, is a good single-ion conducting candidate in future safer Li batteries.

Experimental section

H-Nafion membrane was prepared from the Nafion 5 wt% solution (E.W. 1100, Ion Power Inc, München Germany) according to the following procedure. The Nafion solution

was heated at 80°C to gradually replace the solvents, water and alcohols, with *N,N*-dimethylacetamide (> 99.5%, Sigma Aldrich, St. Louis, MO, USA) at 80°C [39]. Afterwards, the solution obtained was casted on a Petri dish and dried at 80°C overnight. Finally, the membrane was hot-pressed at 50 atm, 175°C for 15 min and was finally activated in boiling 3% w/w hydrogen peroxide (H_2O_2 , 34.5–36.5%, Sigma Aldrich, St. Louis, MO, USA), H_2SO_4 (0.5 M) and distilled water.

A novel one-step casting procedure was developed to prepare a lithiated Nafion (Li-Nafion) membrane. A concentration of 5 wt% of lithium hydroxide (LiOH, Sigma Aldrich), with respect to the dry Nafion content, was dissolved into the commercial Nafion 5 wt% solution (E.W. 1100, Ion Power Inc, München Germany) at 80°C . Subsequently, solvents were replaced with *N,N*-dimethylacetamide and the final mixture was casted on a Petri dish. Compared to the H-Nafion procedure above-described, the Li-Nafion membrane was not hot-pressed and activated.

Micrographs were acquired through scanning electron microscope SEM–EDS VEGA3 TESCAN.

Small-angle X-ray scattering combined with wide-angle X-ray scattering (SAXS-WAXS) measurements have been carried out to understand the Nafion structure after lithiation process. The X-ray scattering measurements were performed at SAXSLabSapienza with a Xeuss 2.0 Q-Xoom system (Xenocs SAS, Grenoble, France), equipped with a micro-focus Genix 3D X-ray Cu source ($\lambda = 0.15419 \text{ nm}$), a two-dimensional Pilatus3 R 300 K detector which can be placed at variable distance from the sample, and an additional Pilatus3 R 100 K detector at fixed shorter distance to access larger scattering angles (Dectris Ltd., Baden, Switzerland). Calibration of the scattering vector q range, where $q = (4\pi \sin\theta)/\lambda$, 2θ being the scattering angle, was performed using silver behenate for the small-angle region and Al_2O_3 for the fixed-distance wide-angle detector. Dried membrane samples (H-Nafion and Li-Nafion) were fixed with tape on the sample holder and placed in the instrument sample chamber at reduced pressure ($\sim 0.1 \text{ mbar}$). The isotropic two-dimensional scattering patterns were subtracted for the “dark” counts, and then masked, azimuthally averaged, and normalized for transmitted beam intensity, exposure time and subtended solid angle per pixel, by using the FoxTrot software developed at SOLEIL. The obtained one-dimensional intensity vs. q profiles in the different angular ranges were merged using the SAXS utilities tool [40] and converted into absolute intensity units (cm^{-1} , macroscopic scattering cross section) dividing by the sample thickness expressed in cm (0.018 cm for H-Nafion and 0.010 cm for Li-Nafion).

Vibrational spectroscopy study was carried out by Attenuated Total Reflectance-Fourier Transform Infrared (ATR-FTIR) to examine molecular interactions and chemical

composition of both H⁺- and Li⁺-Nafion membranes. ATR-FTIR spectra was collected with a PerkinElmer 2000 FT-IR spectrometer in the attenuated total reflection mode using a diamond crystal. The spectral resolution was set to 1 cm⁻¹ recording 264 scans for each sample at room temperature in the range of 400–4000 cm⁻¹. Thermal gravimetric analysis (TGA) was performed with a TGA2 (Mettler-Toledo, Zaventem, Belgium) on dry Nafion membranes under air flux (80 ml/min) in a temperature range between 25 and 550 °C with a scan rate of 5 °C/min. Prior to measurements, the samples were dried at 80 °C under vacuum for 12 h.

For electrochemical characterizations, the membranes were soaked in solvent mixtures containing: ethylene carbonate-propylene carbonate (EC:PC 1:1 w/w), ethylene carbonate-dimethyl carbonate (EC:DMC 1:1 w/w), and ethylene carbonate-diethyl carbonate (EC:DEC 1:1.2 w/w). Before swelling, the membranes were dried at 120 °C under vacuum overnight and placed in an Ar-filled glove box (Jacomex GP(concept)) having a moisture and oxygen content ≤ 1 ppm. The membranes were then immersed in the mentioned solutions, prior the electrochemical measurements.

The ionic conductivity was obtained by electrochemical impedance spectroscopy (EIS) at temperatures of 20 °C, 40 °C and 60 °C by using a ModuLab XM ECS potentiostat, applying a 10 mV amplitude signal in the frequency range 100 kHz–1 Hz. CR2032 coin cell configuration was adopted for these measurements and assembled in a dry glove-box (O₂ and H₂O level below 1 ppm), placing the given electrolyte membrane sandwiched between two carbon paper electrodes and then between two stainless steel current collectors.

The properties of the membrane/lithium metal electrode interface were analyzed by lithium stripping-deposition tests in a symmetrical Li-metal cell. Currents of 0.01 mAcm⁻², 0.05 mAcm⁻² and 0.1 mAcm⁻² were applied for 1 h per single stripping-deposition cycle at 30 °C.

The electrochemical stability window of the membranes was determined by linear sweep voltammetry (LSV) and by cyclic voltammetry (CV) using a Biologic VMP-3e. The measurements were performed by scanning the cell potential from the OCV (open circuit potential) to 6 V vs. Li⁺/Li (anodic stability window, LSV) in a LiLi-Nafion|Super-P carbon-coated Al cell configuration, and from 3 to 0 V vs. Li⁺/Li (cathodic stability window, CV) in a LiLi-Nafion|Super-P carbon-coated Cu cell with a scanning rate of 0.1 mV/s.

Interfacial resistance of Li-Nafion membrane swollen in EC:PC on lithium metal surface was analyzed by electrochemical impedance spectroscopy (EIS) experiments in a symmetric LiLi-Nafion|Li cell. EIS measurements were performed applying a potential of 10 mV in the frequency range of 1 MHz–10 Hz using a Biologic VMP-3e. The impedance

spectra were acquired at the open circuit for 4 days. The obtained Nyquist plots were fitted with ZFit implemented in EC-lab v.11.43 software and they have been described by a R(RQ)(RQ) equivalent circuit. The interfacial resistance was obtained from the sum of the second and the third resistances.

Prototype cells were formed by coupling a lithium metal anode and an olivine-type LiFePO₄ (LFP) cathode with a selected Li-polymer electrolyte membrane. The electrodes were prepared mixing commercial LFP (Sud-Chemie), SuperP carbon and PVdF in a weight ratio of 80/10/10. NMP (*N*-methyl-2-pyrrolidinone) was added as solvent to form a slurry. Then, the as obtained slurry was casted on an aluminium foil with the use of a doctor blade in order to have a thickness of 200 μm. Once dried in oven at 50 °C under vacuum, the coated aluminium foil was calendared and disks with a diameter of 10 mm were cut. The obtained electrodes have a mass loading of LiFePO₄ was 2.02 mg/cm².

Electrodes preparation was performed in a dry room at 20 °C with a Dew Point of – 70 °C.

Before electrochemical tests LFP electrodes were dried under vacuum in a Buchi oven at 110 °C overnight. Swagelok-like two electrodes cell was assembled facing LFP electrode with a foil of metallic lithium, separated by Li-Nafion membrane soaked with EC:PC.

These cells were cycled galvanostatically, by first charging and then discharging, at 30 °C and C/10 rate, using a Maccor Series 4000 battery test system. At the end of each cycle, impedance spectra were recorded by applying a potential of 10 mV in the frequency range of 1 MHz–10 Hz using a ModuLab XM ECS instrument.

Supplementary Information The online version contains supplementary material available at <https://doi.org/10.1007/s40243-023-00249-0>.

Acknowledgements The authors would like to thank Livia Della Seta at ENEA, for SEM images. The Sapienza Research Infrastructure, funded by the Large Equipment Project 2015-C26J15BX54, is acknowledged for the SAXS measurements at SAXS LabSapienza. L.M. thanks Sapienza University of Rome for funding Progetto per Avvio alla Ricerca-Tipo 2, AR22117A5D4153C7. M.A.N. thanks the financial support of the National Recovery and Resilience Plan (PNRR), Mission 4 Component 2 Investment 1.3, funded from the European Union—NextGenerationEU, within the Spoke 6 “Energy Storage” of the Extended Partnership (PE2) NEST—Network 4 Energy Sustainable Transition”.

Declarations

Conflict of interest On behalf of all authors, the corresponding author states that there is no conflict of interest.

Open Access This article is licensed under a Creative Commons Attribution 4.0 International License, which permits use, sharing, adaptation, distribution and reproduction in any medium or format, as long as you give appropriate credit to the original author(s) and the source, provide a link to the Creative Commons licence, and indicate if changes were made. The images or other third party material in this article are

included in the article's Creative Commons licence, unless indicated otherwise in a credit line to the material. If material is not included in the article's Creative Commons licence and your intended use is not permitted by statutory regulation or exceeds the permitted use, you will need to obtain permission directly from the copyright holder. To view a copy of this licence, visit <http://creativecommons.org/licenses/by/4.0/>.

References

1. Chu, S., Majumdar, A.: *Nature* **488**, 294–303 (2012). <https://doi.org/10.1038/nature11475>
2. Tarascon, J.M., Armand, M.: *Nature* **414**, 359–367 (2001). <https://doi.org/10.1038/35104644>
3. Liu, K., Liu, Y., Lin, D., Pei, A., Cui, Y.: *Sci. Adv.* **4**, 1–11 (2018). <https://doi.org/10.1126/sciadv.aas9820>
4. Zhao, W., Yi, J., He, P., Zhou, H.: *Electrochem. Energy Rev.* **2**, 574–605 (2019). <https://doi.org/10.1007/s41918-019-00048-0>
5. Grey, C.P., Hall, D.S.: *Nat. Commun.* **11**, 6279–6283 (2020). <https://doi.org/10.1038/s41467-020-19991-4>
6. Chen, X., He, W., Ding, L.-X., Wang, S., Wang, H.: *Energy Environ. Sci.* **12**, 938–944 (2019). <https://doi.org/10.1039/C8EE02617C>
7. Meyer, W.H.: *Adv. Mater.* **10**, 439–448 (1998). [https://doi.org/10.1002/\(SICI\)1521-4095\(199804\)10:6%3c439::AID-ADMA439%3e3.0.CO;2-I](https://doi.org/10.1002/(SICI)1521-4095(199804)10:6%3c439::AID-ADMA439%3e3.0.CO;2-I)
8. Cai, Z., Liu, Y., Liu, S., Li, L., Zhang, Y.: *Energy Environ. Sci.* **5**, 5690–5693 (2012). <https://doi.org/10.1039/C1EE02708E>
9. Zhang, H., Li, C., Piszcz, M., Coya, E., Rojo, T., Rodríguez-Martínez, L.M., Armand, M., Zhou, Z.: *Chem. Soc. Rev.* **3**, 797–815 (2017). <https://doi.org/10.1039/C6CS00491A>
10. Park, C.H., Sun, Y.-K., Kim, D.-W.: *Electrochim. Acta* **50**, 375–378 (2004). <https://doi.org/10.1016/j.electacta.2004.01.110>
11. Wang, Y., Chen, K.S., Mishler, J., Cho, S.C., Adroher, X.C.: *Appl. Energy* **88**, 981–1007 (2011). <https://doi.org/10.1016/j.apenergy.2010.09.030>
12. Siracusano, S., Oldani, C., Navarra, M.A., Tonella, S., Mazzapioda, L., Briguglio, N., Aricò, A.S.: *J. Membr. Sci.* **578**, 136–148 (2019). <https://doi.org/10.1016/j.memsci.2019.02.021>
13. Zhou, D., Shanmukaraj, D., Tkacheva, A., Armand, M., Wang, G.: *Chem* **5**, 2326–2352 (2019). <https://doi.org/10.1016/j.chempr.2019.05.009>
14. Diederichsen, K.M., McShane, E.J., McCloskey, B.D.: *ACS Energy Lett.* **2**, 2563–2575 (2017). <https://doi.org/10.1021/acsenerylett.7b00792>
15. Jin, Z.Q., Xie, K., Hong, X.B., Hu, Z.Q., Liu, X.J.: *Power Sources* **218**, 163–167 (2012). <https://doi.org/10.1016/j.jpowsour.2012.06.100>
16. Gao, J., Sun, C., Xu, L., Chen, J., Wang, C., Guo, D., Chen, H.: *J. Power. Sources* **382**, 179–189 (2018). <https://doi.org/10.1016/j.jpowsour.2018.01.063>
17. Gao, J., Shao, Q., Chen, J.: *J. Energy Chem.* **46**, 237–247 (2020). <https://doi.org/10.1016/j.jechem.2019.11.012>
18. Fernandez Bordín, S.P., Andrada, H.E., Carreras, A.C., Castellano, G.E., Oliveira, R.G., Galván Josa, V.M.: *Polymers* **155**, 58–63 (2018). <https://doi.org/10.1016/j.polymer.2018.09.014>
19. Mazzapioda, L., Lo Vecchio, C., Danyliv, O., Baglio, V., Martinelli, A., Navarra, M.A.: *Polymers* **12**, 2019–2023 (2020). <https://doi.org/10.3390/polym12092019>
20. Kreuer, K.-D., Portale, G.: *Adv. Funct. Mater.* **23**, 5390–5397 (2013). <https://doi.org/10.1002/adfm.201300376>
21. Nicotera, I., Simari, C., Agostini, M., Enotiadis, A., Brutti, S.: *J. Phys. Chem. C* **123**, 27406–27416 (2019). <https://doi.org/10.1021/acs.jpcc.9b08826>
22. Bauer, I., Thieme, S., Brückner, J., Althues, H., Kaskel, S.: *J. Power. Sources* **251**, 417–422 (2014). <https://doi.org/10.1016/j.jpowsour.2013.11.090>
23. Sachan, S., Ray, C.A., Perusich, S.A.: *Polym. Eng. Sci.* **7**, 1469–1480 (2004). <https://doi.org/10.1002/pen.11044>
24. Sigwadi, R., Dhlamini, M.S., Mokrani, T., Némavhola, F., Nonjola, P.F., Msomi, P.F.: *Heliyon* **5**, 02240–02250 (2019). <https://doi.org/10.1016/j.heliyon.2019.e02240>
25. Austing, J.G., Kirchner, C.N., Komsysiaka, L., Wittstock, G.: *J. Membr. Sci.* **510**, 259–269 (2016). <https://doi.org/10.1016/j.memsci.2016.03.005>
26. Jin, Z., Xie, K., Hong, X.: *J. Mater. Chem.* **1**, 342–347 (2012). <https://doi.org/10.1039/C2TA00134A>
27. Mazzapioda, L., Panero, S., Navarra, M.A.: *Polymers* **11**, 914–924 (2019). <https://doi.org/10.3390/polym11050914>
28. Liang, H.-Y., Qiu, X.-P., Zhang, S.-C., Zhu, W.-T., Chen, L.-Q.: *J. Appl. Electrochem.* **34**, 1211–1214 (2004). <https://doi.org/10.1007/s10800-004-1767-0>
29. Liu, Y., Cai, Z., Tan, L., Li, L.: *Energy Environ. Sci.* **5**, 9007–9013 (2012). <https://doi.org/10.1039/C2EE22753C>
30. Navarra, M.A., Manzi, J., Lombardo, L., Panero, S., Scrosati, B.: *Chemsuschem* **4**, 125–130 (2011). <https://doi.org/10.1002/cssc.2011000254>
31. Sanginov, E.A., Kayumov, R.R., Shmygleva, L.V., Lesnichaya, V.A., Karelin, A.I., Dobrovolsky, Y.A.: *Solid State Ion.* **300**, 26–31 (2017). <https://doi.org/10.1016/j.ssi.2016.11.017>
32. Mayadevi, T.S., Goo, B.-H., Paek, S.Y., Choi, O., Kim, Y., Kwon, O.J., Lee, S.Y., Kim, H.J., Kim, T.H.: *ACS Omega* **7**, 12956–12970 (2022). <https://doi.org/10.1021/acsomega.2c00263>
33. Rahbari, A., Hartkamp, R., Moulτος, O.A., Bos, A., van den Broeke, L.J.P., Ramdin, M., Dubbeldam, D., Lyulin, A.V., Vlucht, T.J.H.: *J. Phys. Chem. C* **126**, 8121–8133 (2022). <https://doi.org/10.1021/acs.jpcc.2c01226>
34. Lim, D.-W., Sadakiyo, M., Kitagawa, H.: *Chem. Sci.* **10**, 16–33 (2019). <https://doi.org/10.1039/C8SC04475A>
35. Voropaeva, D.Y., Novikova, S.A., Kulova, T.L., Yaroslavtsev, A.B.: *Ionics* **24**, 1685–1692 (2018). <https://doi.org/10.3390/batteries8100162>
36. Poiana, R., Lufitano, E., Tsurumaki, A., Simari, C., Nicotera, I., Navarra, M.A.: *Electrochim. Acta* **401**, 139470–139478 (2022). <https://doi.org/10.1016/j.electacta.2021.139470>
37. Tsurumaki, A., Ohno, H., Panero, S., Navarra, M.A.: *Electrochim. Acta* **293**, 160–165 (2019). <https://doi.org/10.1016/j.electacta.2018.09.205>
38. Christmann, K., Friedrich, K.A., Zamel, N.: *Prog. Energy Combust. Sci.* **85**, 100924–100949 (2021). <https://doi.org/10.1016/j.pecs.2021.100924>
39. Mazzapioda, L., Navarra, M.A., Trequattrini, F., Paolone, A., Elamin, K., Martinelli, A., Palumbo, O.: *Membranes* **9**, 143–155 (2019). <https://doi.org/10.1007/s10008-021-05025-6>
40. Sztucki, M., Narayanan, T.: *J. Appl. Cryst.* **40**, s459–s462 (2007). <https://doi.org/10.1107/S002188980604583>

Publisher's Note Springer Nature remains neutral with regard to jurisdictional claims in published maps and institutional affiliations.